Available online at www.sciencedirect.com
ScienceDirect
Acta Materialia 55 (2007) 5859–5866
Acta MATERIALIA
www.elsevier.com/locate/actamat

Arrest, deflection, penetration and reinitiation of cracks in brittle layers across adhesive interlayers

James Jin-Wu Lee [a], Isabel K. Lloyd [a], Herzl Chai [b], Yeon-Gil Jung [c], Brian R. Lawn [d,*]

[a] Department of Materials Science and Engineering, University of Maryland, College Park, MD 20742-2115, USA
[b] Department of Solid Mechanics, Materials and Systems, Tel Aviv University, Tel Aviv, Israel
[c] School of Nano and Advanced Materials Engineering, Changwon National University, Changwon, Kyung-Nam, South Korea
[d] Materials Science and Engineering Laboratory, National Institute of Standards and Technology, Gaithersburg, MD 20899-8520, USA

Received 9 January 2007; received in revised form 27 June 2007; accepted 28 June 2007
Available online 21 August 2007

Abstract

A layer structure consisting of two glass plates bonded with polymer-based adhesives and loaded at the upper surface with a line-wedge indenter is used to evaluate crack containment. Two adhesives are used, a low-modulus epoxy resin and a particle-filled composite. The adhesives arrest indentation-induced transverse cracks at the first interface. A substantially higher load is required to resume propagation beyond the second interface in the second glass layer. Delamination is not a principal failure mode. Nor is the operative mode of failure one of continuous crack penetration through the adhesive, but rather reinitiation of a secondary crack in the glass ahead of the arrested primary crack. A fracture mechanics analysis, in conjunction with finite element modeling, is presented to account for the essential elements of crack inhibition, and to identify critical material and layer thickness variables. It is confirmed that adhesives with lower modulus and higher thickness are most effective as crack arresters.
Published by Elsevier Ltd on behalf of Acta Materialia Inc.

Keywords: Adhesive joining; Glass; Contact loading; Crack containment; Crack penetration

1. Introduction

Polymer-based adhesives provide a simple means of joining adjacent brittle layers at room temperature, thereby avoiding the serious residual stresses from differentials in coefficient of thermal expansion that can accompany fusion-bonding processes. Adhesive bonds are relevant to functional structures such as car windshields and laminates [1–7]. They also offer a potential means for fabricating dental crowns, by joining porcelain veneers to core ceramics [8]. Goals for such adhesives include: (i) provide strong bonding to impede any transverse cracks formed within the brittle layers at the adhesive interface, without delamination; (ii) make the adhesive sufficiently compliant, so as to shield adjacent layers from applied loading [9]; and (iii) make the adhesive sufficiently stiff, to avoid flexure of the upper the layer and thus circumvent the incidence of secondary failure modes [6]. Clearly, the design of optimal layer structures of this kind involves some compromises in properties matching.

At issue here is the behavior of transverse cracks when they approach such an adhesive interlayer. Transverse cracks may initiate at one surface in tension or bending or, more frequently, in concentrated top-surface loading [6,10–12]. Once any such crack has traversed a single brittle layer and arrested at the first adhesive interface, various possibilities exist for further advance in overload: delaminate at the first or second interface (deflection) [13–15]; extend progressively through the adhesive into the adjacent brittle layer (penetration); or reinitiate ahead of the crack tip in the adjacent brittle layer (reinitiation) [9]. This raises a number of questions. What determines which of these modes prevails? What is the role of key material properties

* Corresponding author. Tel.: +1 301 975 5775.
E-mail address: brian.lawn@nist.gov (B.R. Lawn).

1359-6454/$30.00. Published by Elsevier Ltd on behalf of Acta Materialia Inc.
doi:10.1016/j.actamat.2007.06.038

of the adhesive – modulus, toughness, strength, hardness – relative to the adjacent brittle layers? What is the role of adhesive thickness relative to that of the brittle layers?

Here we consider the fracture mechanics of an adhesively bonded model layer system fabricated specifically to address these questions [6,10]. Glass plates are joined with epoxy resin interlayers of specified thicknesses. An indenting wedge is loaded at the surface of the top glass layer to introduce and propagate a line crack through the system. Progress of the crack is monitored directly during indentation by side viewing. This test configuration has the advantage of being particularly simple, with highly stable cracks. It is also amenable to plane strain fracture mechanics, thus providing a theoretical basis for characterization of adhesive properties.

2. Fracture mechanics: penetration vs. reinitiation

2.1. General mechanics

Consider the test configuration in Fig. 1. A brittle plate (material 1) of thickness d, modulus E_1, toughness T_1 and strength S_1 is bonded with adhesive (material 2) of thickness h, modulus E_2 and toughness T_2 to a like brittle base plate (material 1) of thickness $\gg d$. A wedge indenter under line load $P_l = P/l$ along a specimen width l introduces a transverse plane crack of depth c within the upper plate, and drives this crack downward to the adhesive interface. The action of the indenter will generally induce a near-field contact plastic zone, responsible for nucleating the crack in the first place and augmenting the elastic driving force in the initial propagation stage [16].

Suppose that the crack reaches the first adhesive interface, and that the bonding is strong enough that delamination does not occur. There are two possibilities for subsequent growth: (i) the crack penetrates into the adhesive, ultimately reaching and entering the second brittle layer; and (ii) after arresting at the first interface or penetrating part way into the adhesive, the crack reinitiates in the second brittle layer ahead of the primary tip. These two modes may be expected to have different dependencies on material and geometrical (thickness) variables.

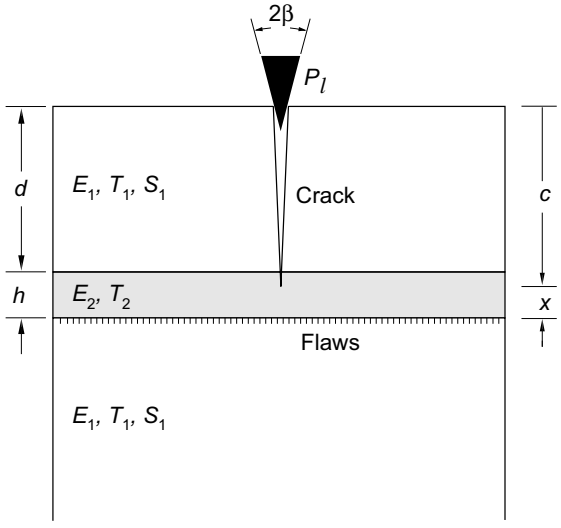

Fig. 1. Schematic of line force crack configuration in a layer system consisting of two brittle plates bonded by a polymer-based adhesive. The crack can propagate into the lower brittle layer either by continuous penetration or reinitiation from a surface flaw ahead of an arrested primary crack tip.

2.2. Crack penetration

Crack penetration might be expected to be the principal mode for adhesives that are relatively stiff, hard and brittle. Begin with a simple relation for a thick monolithic brittle specimen of material 1, and then modify to allow for presence of an intervening adhesive material 2. Assuming the principal driving force to come from the horizontal component of the applied line force, the stress intensity factor for such a crack may be written [16–18] as

$$K_0 = \alpha P_l/[(\pi c)^{1/2}\tan\beta'] = \chi_e P_l/c^{1/2} \quad (1)$$

where $\beta' = \beta + \arctan\mu$ is an effective indentation wedge half-angle, with β the true wedge half-angle and μ a friction coefficient, and α and $\chi_e = \alpha/\pi^{1/2}\tan\beta'$ dimensionless constants. This relation ignores any influence from the vertical line force component on the crack growth, but any such contribution may be subsumed into α and χ_e in Eq. (1). For a layer system with an adhesive interlayer we may write

$$K = \phi K_0 \quad (2)$$

where $\Phi = \Phi(c/d, h/d, E_2/E_1, \nu_2/\nu_1)$ is a dimensionless function defining the influence of the interlayer, with E Young's modulus and ν Poisson's ratio. (Note the limiting case $\Phi = 1$ for a brittle monolith, $E_1 = E_2$ and $\nu_2 = \nu_1$). The function Φ for any given ratio E_2/E_1 can be evaluated by two-dimensional finite element modeling (FEM) by emplacing cracks of length c in structures with and without adhesive interlayers (Fig. 1) using the Irwin crack-opening displacement relation [19] to compute relative stress intensity factors at any given load Pl and crack size c [20]. A supplementary benefit of FEM analysis is to confirm that stress components in our system remain within the elastic limit, a necessary condition for validity of the fracture mechanics formalism.

Results of FEM calculations of the function Φ as a function of relative crack size c/d are shown in Fig. 2 for a set of experimental conditions to be described in the next section, using ANSYS software (Version 6.0, ANSYS Inc., Cannonsburg, PA). The FEM system comprises upper and lower glass plates with an interlayer adhesive of relative modulus $E_2/E_1 = 0.22$ or 0.040 and relative thickness $h/d = 0.05$. Lateral dimensions for the system are $80d$, large enough to eliminate any boundary effects. Values of material parameters inserted into the FEM code are listed in Table 1. Forces are applied at the crack mouth with an indenter of rectangular cross-section (i.e. $\beta = 45^\circ$). The

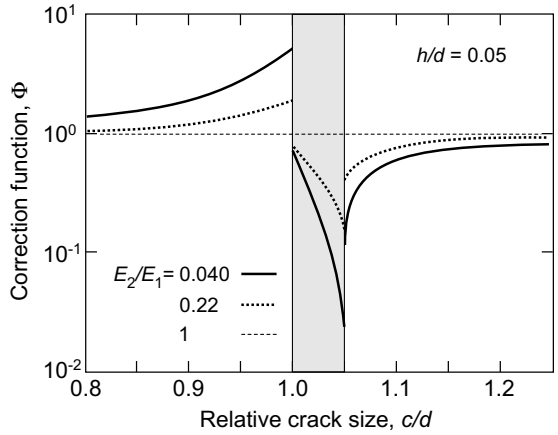

Fig. 2. Plot of function $\Phi(c/d)$ for brittle plates bonded with adhesives of relative thickness $h/d = 0.05$ and modulus $E_2/E_1 = 0.040$ and 0.22.

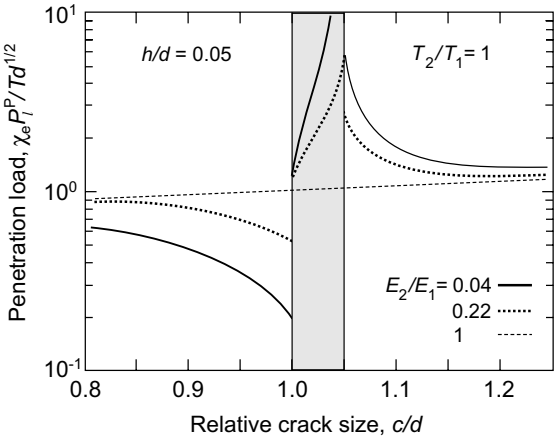

Fig. 3. Plot of $\chi_e P_l^P/Td^{1/2}$ vs. c/d for given h/d and E_2/E_1.

Table 1
Parameters for materials in this study

Material	E (GPa)	ν	T (MPa m$^{1/2}$)	S (MPa)
Glass (abraded)	73	0.22	0.6	115
Glass (etched)	73	0.22	0.6	300
Epoxy	2.9	0.35	1.0	–
Composite	16	0.35	1.0	–

E = Young's modulus, ν = Poisson's ratio, T = toughness, S = strength.

mesh is refined until solutions converge. The plots in Fig. 2 indicate a modestly rising crack attraction on approaching the first interface ($\Phi > 1$), a pronounced crack inhibition within the compliant adhesive layer ($\Phi \ll 1$) and continued (but reduced) crack inhibition beyond the second interface ($\Phi < 1$). The positive deviations from unity in the first region are similar to those calculated for cracks approaching and crossing the interface between a stiff coating and compliant substrate in a simple bilayer [21]. The negative deviations in the second and third regions reflect the degree of stress shielding exerted by the adhesive on the crack propagation. Note the greater shielding effect in layers with greater mismatch, i.e. smaller E_2/E_1.

The condition for equilibrium crack penetration at any given length c can be determined by equating the stress intensity factor K to the appropriate toughness T (K_{IC}). Using superscript P to denote penetration mode, Eqs. (1) and (2) then yield

$$P_l^P = (Td^{1/2}/\chi_e)[(c/d)^{1/2}/\Phi(c/d)] \quad (3)$$

where $T = T_1$ within $c < d$, $T = T_2$ within $d < c < d + h$ and $T = T_1$ within $c > d + h$. Note P_l^P is independent of strength of the brittle materials – it is toughness that controls the crack growth in this mode.

To illustrate, P_l^P in Eq. (3) is plotted in normalized form in Fig. 3 as a function of c/d, using $\Phi(c/d)$ from Fig. 2. For this case we take $T_2 = T_1$, to emphasize the modulus mismatch shielding effect. Note the monotonically increasing function for monoliths ($E_2/E_1 = 1$, $\nu_2 = \nu_1$). For $E_2/E_1 < 1$, $P(c)$ actually passes through a maximum at $c \approx 0.5d$, corresponding to a small pop-in to the interface, the more pronounced for lower E_2/E_1. Thereafter, within $d < c < d + h$, a substantial load increment is required to drive the crack through the adhesive, and the fracture becomes highly stable. The requirement in Eq. (3) for the crack to reach the second interface at $c_* = d + h$ is defined by a "penetration function"

$$P_l^P(c_*) = (T_2 d^{1/2}/\chi_e)[(1 + h/d)^{1/2}/\Phi(c_*/d)] \quad (4)$$

At this point the condition for propagating the crack into the second brittle layer is exceeded and fracture is spontaneous. Of course, such failure assumes that the load $P_l^P(c_*)$ is achieved before fracture occurs by any competing mode.

2.3. Crack reinitiation

In this case, a secondary crack initiates in the lower brittle layer within the K-field of the primary crack prior to penetration to the second interface. This is the expected mode for adhesives that are relatively compliant, soft and tough. Simplistically, the condition for reinitiation is that the maximum tensile stress in the near-surface of the second brittle layer just equals the strength $S_1 = T_1/(\pi c_f)^{1/2}$ of that layer, where c_f is a characteristic flaw size. This condition ignores any effects of crack tip stress gradients over the critical flaw, which could be substantial in the region $h < c_f$. Designating the distance ahead of the primary crack tip as $x = d + h - c$ (Fig. 1), the normal stress at the surface of the second brittle layer can be approximated by [9]

$$\sigma_y = K_0/(2\pi x)^{1/2} \quad (5)$$

within the region $x \ll c + h$. It is implicit in this relation that the intervening adhesive layer does not seriously perturb the K field in the second brittle layer (regardless of whether the crack resides in the first brittle layer or the adhesive layer). Inserting $\sigma_y = S_1$ along with $x = d + h - c$ in Eq. (5) then yields a "reinitiation function"

$$P_l^I = (S_1 d/\chi_e)[(2\pi c/d)(1 + h/d - c/d)]^{1/2} \quad (6)$$

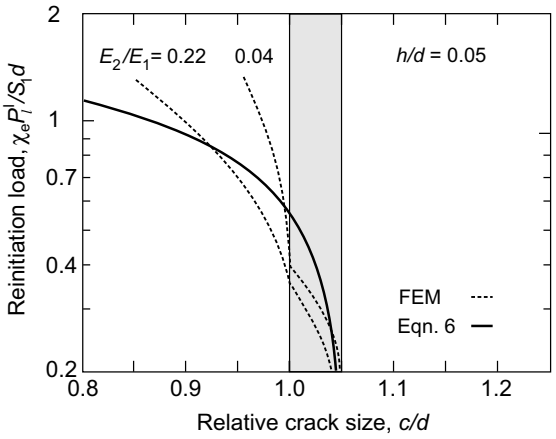

Fig. 4. Plot of $\chi_e P_l^I/S_1 d$ vs. c/d for given h/d.

Note that it is now strength and not toughness of the second layer that determines the critical condition. Note also that P_l^I is independent of E_2/E_1 in this approximation. Again, justification of the assumptions and approximations used in the derivation of Eq. (6) requires numerical verification.

A plot of the normalized reinitiation load P_l^I as a function of relative crack size c/d, for relative thickness $h/d = 0.05$ is shown in Fig. 4. The solid line is a direct representation of Eq. (6), the dashed lines are FEM calculations for $E_2/E_1 = 0.22$ and 0.040 with a calibrated coefficient $\chi_e = 0.21$ (see Section 4.2). The FEM curves deviate from Eq. (6) in the region $c < d$, which lies outside the range of validity of the Irwin crack-tip field. However, in the vicinity of the adhesive Eq. (6) provides a fair representation of the critical conditions. The probability of reinitiation increases dramatically as the primary crack approaches the second interface. Once the condition for reinitiation is met, the crack pops in from a critical flaw in the surface of the lower brittle layer.

A special case of interest is that of reinitiation in the field of an arrested primary crack at the first interface. Inserting $c_* = d$ into Eq. (6) yields

$$P_l^I(c_*) = (S_1 d/\chi_e)(2\pi h/d)^{1/2} \tag{7}$$

This relation emphasizes the role of interlayer thickness h in the reinitiation process.

The issue of which mode wins, penetration or reinitiation, is then determined by the relative values of P_l^P in Eq. (3) and P_l^I in Eq. (6).

3. Experiment

Soda-lime glass plates were chosen as model brittle layers. Glass is isotropic and homogeneous, easy to prepare and amenable to in situ observations during indentation [6,10,22]. Plates of thickness $d = 1$ mm, width 3 mm and length 25 mm were used for the upper layer. Blocks of thickness 12.5 mm and minimum lateral dimensions 25 mm were used as lower layers, as well as monoliths for control experiments. Prior to bonding, the top surface of the lower plates were either abraded (grade 600 SiC grit) to introduce a uniform density of starter flaws for reinitiation, or etched (10% HF, 30 s) to remove any existing flaws. From earlier studies, this produced surfaces with characteristic flexural strengths $S_1 = 115$ MPa (abraded) and $S_1 = 300$ MPa (etched) [10] (Table 1).

The upper and lower glass plates were then bonded with either of two polymer-based adhesives: (i) epoxy resin (Harcos Chemicals, Bellesville, NJ), cured for 1 day at room temperature; or (ii) 72% by mass filled-composite resin [23], consisting of 45 nm spherical alumina particles (NanoTek, Nanophase Technologies Corp., Romeoville, IL) in a monomer blend of 50 mass% bisphenol-A-glycidyldimethacrylate (*bis*-GMA, Esstech, Essington, PA) and 50 mass% triethylene glycol dimethacrylate (TEDGMA, Sigma-Alrich, St. Louis, MO), pre-stirred for 4 h and cured at 120 °C for 6 h. The glass surfaces were first silanized (3M ESPE RelyX Ceramic Primer, St. Paul, MN) to enhance chemical bonding. Spacers between the glass plates were used to predetermine the adhesive thickness, most commonly $h = 50$ μm but others in the range $h = 1$ μm to 1 mm. Modulus values for each adhesive were determined from nanoindentation experiments. Again, values are included in Table 1.

Rectangular tungsten carbide (WC) insert blocks used in glass cutters (Wale Apparatus Co., Hellertown, PA) of edge sharpness <10 μm and length 40 mm (i.e. much larger than the specimen width 3 mm) were used as line indenters. These were mounted into a v-notch in the crosshead platten of a mechanical testing machine, with the indenter faces at angle 45° to the upper glass surface and with the contacting edge carefully aligned along the specimen width. All tests were conducted in air, and the load rate adjusted to drive the crack through the adhesive interlayer for a period of about 1 min. A video camera was used to monitor the crack growth side-on during loading through the entire fracture process. The resolution of this viewing instrument was sufficient to follow the progress through the two glass layers, but not within the thinner adhesive interlayers. In the latter case, specimens with cracks arrested at the first interface were viewed in interrupted tests using high-magnification microscopy.

4. Results

4.1. Crack morphology

Fig. 5 shows a video sequence of a line-indentation crack in a layer structure with particulate-composite adhesive, upper glass thickness $d = 1$ mm and adhesive thickness $h = 50$ μm, and with top surface of the lower glass layer abraded. The crack is shown propagating somewhat unstably with monotonically increasing line load P_l in Fig. 5a and b, to interfacial arrest at $P_l \approx 54$ N mm^{-1} in Fig. 5c. A substantially higher load, $P_l \approx 133$ N mm^{-1}, is required to pop the crack into the lower glass layer in

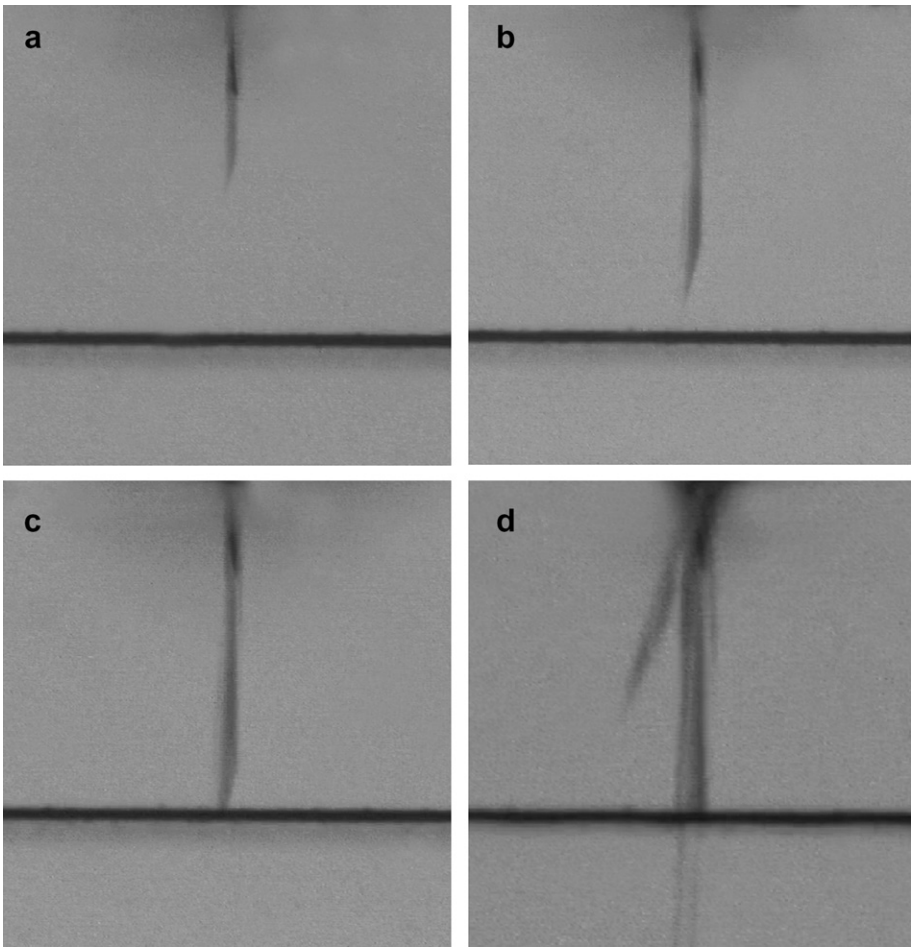

Fig. 5. Video sequence of cracks propagating through a glass/composite-adhesive/glass interface. Thickness of the glass plate and the adhesive are $d = 1$ mm and $h = 50$ μm. The top surface of lower glass plate is abraded. Line force loads P_I are: (a) 52 N mm^{-1}, (b) 53 N mm^{-1}, (c) 54 N mm^{-1} and (d) 133 N mm^{-1}. The load gap between (c) and (d) is an indicator of the crack containment capacity of the interlayer.

Fig. 5d. A higher magnification micrograph of a separate test in which the top surface of the lower glass layer was etched rather than abraded reveals significant crack penetration into the adhesive in Fig. 6. However, in none of this set of specimens, either abraded or etched, did the penetrating crack reach the second interface prior to failure, confirming a dominant reinitiation mode. Note that the cracks in the upper and lower glass layers in Fig. 5d are closely colinear, suggesting that the primary crack has no difficulty locating a critical surface flaw at the location of maximum K-field tensile stress in the abraded lower glass plate.

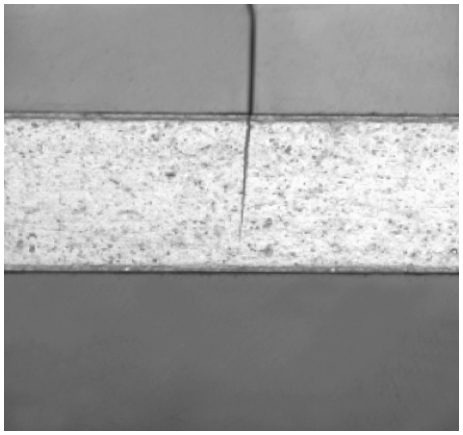

Fig. 6. Similar system to Fig. 5, with composite adhesive thickness $h = 50$ μm, showing a higher-magnification optical micrograph of crack penetration from the upper glass layer into the interlayer.

Analogous observations were made for specimens with epoxy adhesives of the same dimensions as in Fig. 5 and still with abraded lower glass plates. In these specimens, initial crack growth to the first interface was comparable to that in Fig. 5a–c. However, no detectable penetration into the epoxy, of the kind seen in Fig. 6, could be detected prior to failure of the lower brittle layer. Moreover, failure occurred at slightly higher applied loads. These observations indicate enhanced shielding from the epoxy interlayer, and reconfirm dominance of the reinitiation mode.

Additional tests on composite-bonded specimens, again with the same dimensions but with top surface of the lower glass layer etched instead of abraded, showed similar initial crack growth to the first interface, but a different response thereafter. Failure in the lower glass plate now occurred in a much more catastrophic manner and at much higher

applied loads – typically well in excess of $P_I \approx 400$ N mm^{-1} – with fragmentation of the specimen accompanied by delaminations along the adhesive interface. Crack penetrations into the composite layer (but still not in the epoxy) were somewhat deeper but still did not reach the second interface prior to failure, once more consistent with a dominant reinitiation process. Spurious chipping around the indentation site at the top surface sometimes led to load drops in this set of experiments, making determination of critical failure loads somewhat more erratic.

4.2. Fracture mechanics analysis of crack propagation data

A first step in the fracture mechanics analysis was to "calibrate" the coefficients α, μ and χ_e in Eq. (1). This was done using indentation tests on glass monoliths. Filled-symbol data for P_I as a function of crack size c are shown in Fig. 7 for three separate cracks. The solid line is a best fit of Eq. (2) and FEM predictions, yielding $T_1/\chi_e = 2.88$ MPa. Inserting $T_1 = 0.6$ MPa m$^{1/2}$ for glass (stress intensity factor for crack propagation in air, with due allowance for modest slow crack growth [24]) yields $\chi_e = 0.21$. Open-symbol data are FEM calculations, adjusting $\mu = 0.12$ to best fit the solid curve, yielding $\alpha = 0.47$. We may now use these coefficients as input parameters for the layer structures.

Corresponding $P_I(c)$ plots for layer structures of upper glass thickness $d = 1$ mm and abraded lower glass top surface are shown in Fig. 8 for (a) epoxy and (b) composite adhesive interlayers of thickness $h = 50$ μm. Solid curves are predictions from the penetration function $P_l^{\mathrm{P}}(c)$ in Eq. (3), using a generic toughness $T_2 = 1.0$ MPa m$^{1/2}$ for both adhesive materials. (Different toughness values simply scale the $P_l^{\mathrm{P}}(c)$ curves vertically in Fig. 8). Dashed curves are predictions from the reinitiation function $P_l^{\mathrm{I}}(c)$ in Eq. (6), using $S_1 = 115$ MPa for abraded glass. The crossover points between the $P_l^{\mathrm{P}}(c)$ and $P_l^{\mathrm{I}}(c)$ curves within the adhesive layers represent the predicted instability configuration for reinitiation in the second glass layer. (Note in Fig. 8 that these crossovers occur well before the penetration curve intersects the second interface, again consistent with a dominant reinitiation process.) Data points are experimental measurements from video sequences of the kind in Fig. 5 with arrows designating crack instabilities. Critical loads lie in the range 100–200 N mm^{-1} for composite and 200–300 N mm^{-1} for epoxy adhesives. The qualitative crack growth trends observed experimentally are all reproduced by the fracture mechanics analysis, even though the scatter in experimental data is too great and the gradients in the predicted $P_l^{\mathrm{P}}(c)$ and $P_l^{\mathrm{I}}(c)$ curves within the adhesive layer too steep to claim accurate quantitative agreement.

Analogous tests for specimens with the same dimensions but etched bottom glass layers show similar trends (not shown in Fig. 8), but with an upward shift in the $P_l^{\mathrm{I}}(c)$ curves (because of the higher strength value for etched surfaces, $S_1 = 300$ MPa). Critical loads well in excess of 400 N mm^{-1} were observed in failure tests, i.e. substantially higher than for their abraded surface counterparts. Even higher loads might be achieved if the etched speci-

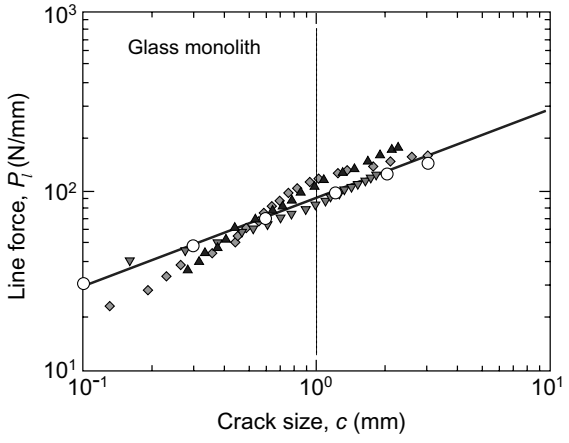

Fig. 7. Line force load P_I as a function of crack size c for monolithic glass. Filled-symbol data are experimental results for three separate cracks. The solid line is a fit of Eq. (1). Open-symbol data are FEM calculations.

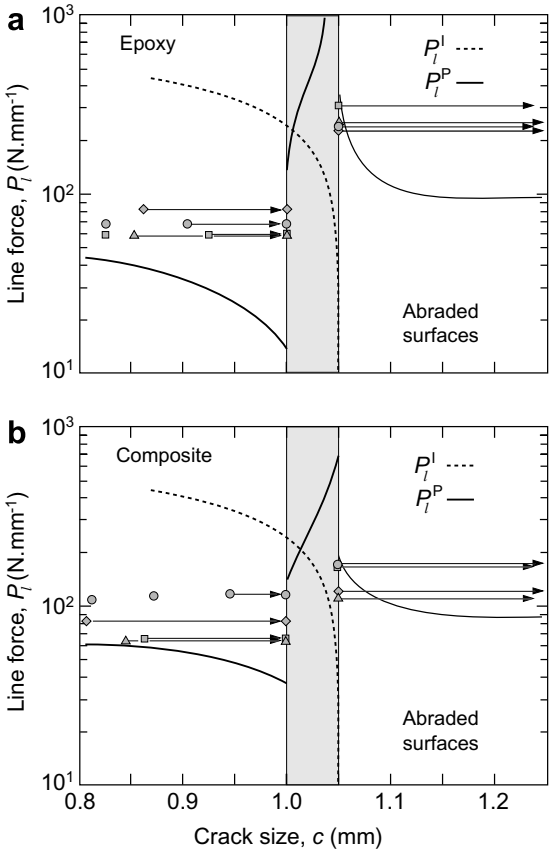

Fig. 8. Line force load P_I as a function of crack size c for glass layer systems: (a) epoxy and (b) particle-filled composite interlayers. Thicknesses $d = 1$ mm and $h = 50$ μm; top surface of the lower glass layer abraded. Data points represent measurements from video sequences. Arrows indicate instabilities in the crack extension. Solid lines are fits of crack penetration function $P_l^{\mathrm{P}}(c)$ in Eq. (3), dashed lines of crack reinitiation function $P_l^{\mathrm{I}}(c)$ in Eq. (6).

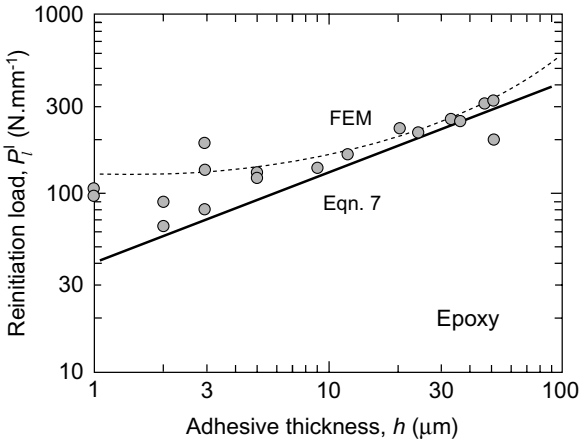

Fig. 9. Critical line force load for crack reinitiation in lower glass layer bonded with epoxy adhesive, as function of adhesive thickness h ($d = 1$ mm).

mens were not to incur spurious handling flaws during fabrication, or if spurious chipping were not to occur.

Critical reinitiation loads for specimens with fixed upper glass layer thickness $d = 1$ mm and abraded bottom glass layers are plotted in Fig. 9 as a function of thickness h, for epoxy interlayers. The solid line is a prediction from the limiting Eq. (7) (which assumes zero crack penetration into the adhesive). The dashed line is a refined FEM calculation taking into account the effects of any stress gradients over a critical (fully embedded) flaw of length $c_f = (2/\pi)(T_1/S_1)^2 \approx 18$ μm (assumed fully embedded, hence factor 2). Note the divergence of the FEM calculation from Eq. (7) at small h, indicating some influence of stress gradients over the flaw length for ultrathin interlayers. Note a divergence also at large h, in this case arising from breakdown of the Irwin K-field relation in Eq. (5). Experimental data points follow the FEM trends to good approximation. These results indicate a relatively slow variation of P_l^I with adhesive thickness, especially in the lower h region.

5. Discussion

The present study has considered how arrested transverse cracks at adhesive interfaces in brittle layers may grow into adjacent brittle layers by either of two mechanisms: penetration of a primary crack through the adhesive or reinitiation ahead of the primary crack in the adjacent layer. A model test configuration consisting of glass plates bonded by epoxy or particulate-filled polymeric adhesives, loaded at the top surface of the upper plate with a line-force indenter, has been used to demonstrate the competition between these two modes. Fracture mechanics and FEM calculations have been used to provide a theoretical basis for analysis. The indenter initially drives a line crack through the upper plate toward the first adhesive interface, at which point arrest occurs. A substantial increase in applied load is then required to drive the crack through the adhesive and into the lower brittle layer. Effectively, the adhesive "shields" the lower layer from the applied load. Direct observation indicates that fracture in the lower brittle layer occurs by reinitiation rather than by continuous penetration, at least for the systems studied here. Fracture mechanics provides qualitative confirmation for the dominance of the reinitiation mode, and usefully identifies the material and layer thickness variables that control the critical loads for failure.

The results highlight the effectiveness of adhesive interlayers as a means of damage containment, by suppressing crack penetration to the point that failure occurs by reinitiation. Lower modulus interlayers are most effective in this regard, providing greater stress shielding (via the Φ term in Eq. (3); Fig. 2). However, even systems with particle-filled composite adhesives are subject to a dominant reinitiation mode in our experiments. The results also highlight the manner in which surface abrasion flaws in the lower glass plate promote the reinitiation mode (via the strength term S_1 in Eq. (6)). Of course, there are limits to the effectiveness of these approaches in suppressing crack penetration, namely where the adhesive modulus approaches that of the brittle layer (equivalent to depressing the $P_l^P(c)$ curves in Fig. 8) and the strength of the adjacent brittle layer is elevated to uncommonly high levels by total removal of surface flaws (equivalent to elevating the $P_l^I(c)$ curves in Fig. 8). In such limiting cases the layer system effectively behaves as a monolith, with continuous crack extension across a virtual interface.

We would point out that penetration and reinitiation are not the only possible fracture modes in adhesively bonded brittle structures of the kind described here. Repeated mention has been made of delamination, and, indeed, that is the most widely studied of all failure modes in layer structures in the fracture literature. Delamination depends primarily on the toughness of the bonding interface relative to that of the bulk brittle layer [14]. Special efforts have been made to minimize delamination in our experiments by silanizing the glass surfaces before bonding. Nevertheless, some debonding was observed in the tests on glass layers with etched surfaces. Another kind of fracture commonly observed in brittle layer structures in concentrated surface loading is radial cracking at the bottom instead of the top surface of the upper glass layer, from flexure of the plate on the compliant adhesive [6–8]. This mode becomes more likely the blunter the indenter (suppressing top-surface cracking), the thinner the brittle plate and the more compliant and thicker the adhesive (enhancing flexure and counteracting the shielding benefit). In other specimen configurations with less concentrated loading, i.e. specimens subjected to constant tensile strain across the section [9], shielding from the applied loading will be less effective and reinitiation therefore more pronounced.

Finally, a comment may be made about the relevance of the present analysis to one practical application: the manufacture of all-ceramic dental crowns. The idea being mooted is that aesthetic porcelain veneers and stiff and strong ceramic cores might be fabricated separately and

then bonded with strong polymeric adhesive at room temperature, replacing the current time-consuming layer-by-layer porcelain fusion processes. Such an alternative route offers several attractive advantages: the bonding process is relatively easy; it promises crack containment, so that a damaged crown might still function until replacement; deleterious thermal mismatch residual stresses would be avoided (although some lesser stresses might arise from the adhesive by shrinkage during curing, or expansion stresses from subsequent absorption of moisture); and the potential exists for some of the adhesive to enter surface flaws and thereby bond fissure walls, increasing strength [25]. As indicated above, the requirements for such a system are stringent – the adhesive needs to be sufficiently compliant and thick to resist crack penetration and reinitiation, but not to the extent that veneer radial cracking is promoted; surface flaws in the surfaces of both core and veneer need to be minimized by careful handling during preparation, to inhibit reinitiation; and with polymeric materials, delamination and accumulation of damage by fatigue always remains a threat.

Acknowledgements

This work was supported by a grant from the US National Institute of Dental and Craniofacial Research (PO1 DE10976) and by NIST internal funds. Certain equipment, instruments or materials are identified in this paper in order to specify experimental details. Such identification does not imply recommendation by the National Institute of Standards and Technology, nor is it meant to imply that the materials are the best available for the purpose.

References

[1] Ball A. J Phys IV 1997;7:C3921.
[2] Grant PV, Cantwell WJ, McKenzie H, Corkhill P. Int J Impact Eng 1998;21:737.
[3] Grant PV, Cantwell WJ. J Test Eval 1999;27:177.
[4] Bennison SJ, Jagota A, Smith CA. J Am Ceram Soc 1999;82:1761.
[5] Maekawa I, Sudou H, Uda K. Int J Impact Eng 2000;24:673.
[6] Chai H, Lawn BR. J Mater Res 2000;15:1017.
[7] Kim JH, Miranda P, Kim DK, Lawn BR. J Mater Res 2003;18:222.
[8] Lee J, Wang Y, Lloyd IK, Lawn BR. J Dent Res 2007;86:745.
[9] Shaw MC, Marshall DB, Dadkhah MS, Evans AG. Acta Metall 1993;41:3311.
[10] Chai H, Lawn BR, Wuttiphan S. J Mater Res 1999;14:3805.
[11] Lawn BR, Deng Y, Miranda P, Pajares A, Chai H, Kim DK. J Mater Res 2002;17:3019.
[12] Bhowmick S, Meléndez-Martínez JJ, Zhang Y, Lawn BR. Acta Mater 2007;55:2479.
[13] Clegg WJ, Kendall K, Alford NM, Button TW, Birchall JD. Nature 1991;347:455.
[14] He M-Y, Hutchinson JW. Int J Solids Struct 1989;25:1053.
[15] Kim J-W, Bhowmick S, Hermann I, Lawn BR. J Biomed Mater Res 2006;79B:58.
[16] Symonds BL, Cook RF, Lawn BR. J Mater Sci 1983;18:1306.
[17] Lawn BR, Fuller ER. J Mater Sci 1975;10:2016.
[18] Lawn BR. Fracture of brittle solids. Cambridge: Cambridge University Press; 1993.
[19] Rooke DP, Cartright DJ. Compendium of stress intensity factors. Uxbridge: Hillingdon Press; 1976.
[20] Chai H. Int J Solids Struct 2003;40:591.
[21] Fett T, Munz D. Stress intensity factors and weight functions. Southampton: Computational Mechanics Publications; 1997.
[22] Chai H, Lawn BR. Acta Mater 2002;50:2613.
[23] Wang Y, Lee JJ, Lloyd IK, Wilson OC, Rosenblum M, Thompson VP. J Biomed Mater Res 2007;82A:651.
[24] Chai H, Lawn BR. Acta Mater 2007;55:2555.
[25] Kim H-W, Deng Y, Miranda P, Pajares A, Kim DK, Kim H-E, et al. J Am Ceram Soc 2001;84:2377.